Numerical Astrodynamics

Assignment I

Lorenz Veithen

TU Delft

DELFT UNIVERSITY OF TECHNOLOGY

FACULTY OF AEROSPACE ENGINEERING

AE4868-1

NUMERICAL ASTRODYNAMICS

Numerical Propagation of JUICE

Lecturer: Dr. D. Dirkx and Dr. Ir. K.J. Cowan

Github repository link:
https://github.com/LorenzVeithen/NumericalAstrodynamics2023_Veithen_Lorenz

March 12, 2023

Q1	Q2	Q3	Q4	Q5
3h	7h	5h	13h	9h

Lorenz Veithen 5075211

Cooperating Students: Srujan Vaidya (5072034) and Oliver Ross (5008042)

TU Delft Delft University of Technology

Problem 1

1.1 Change in Keplerian Elements

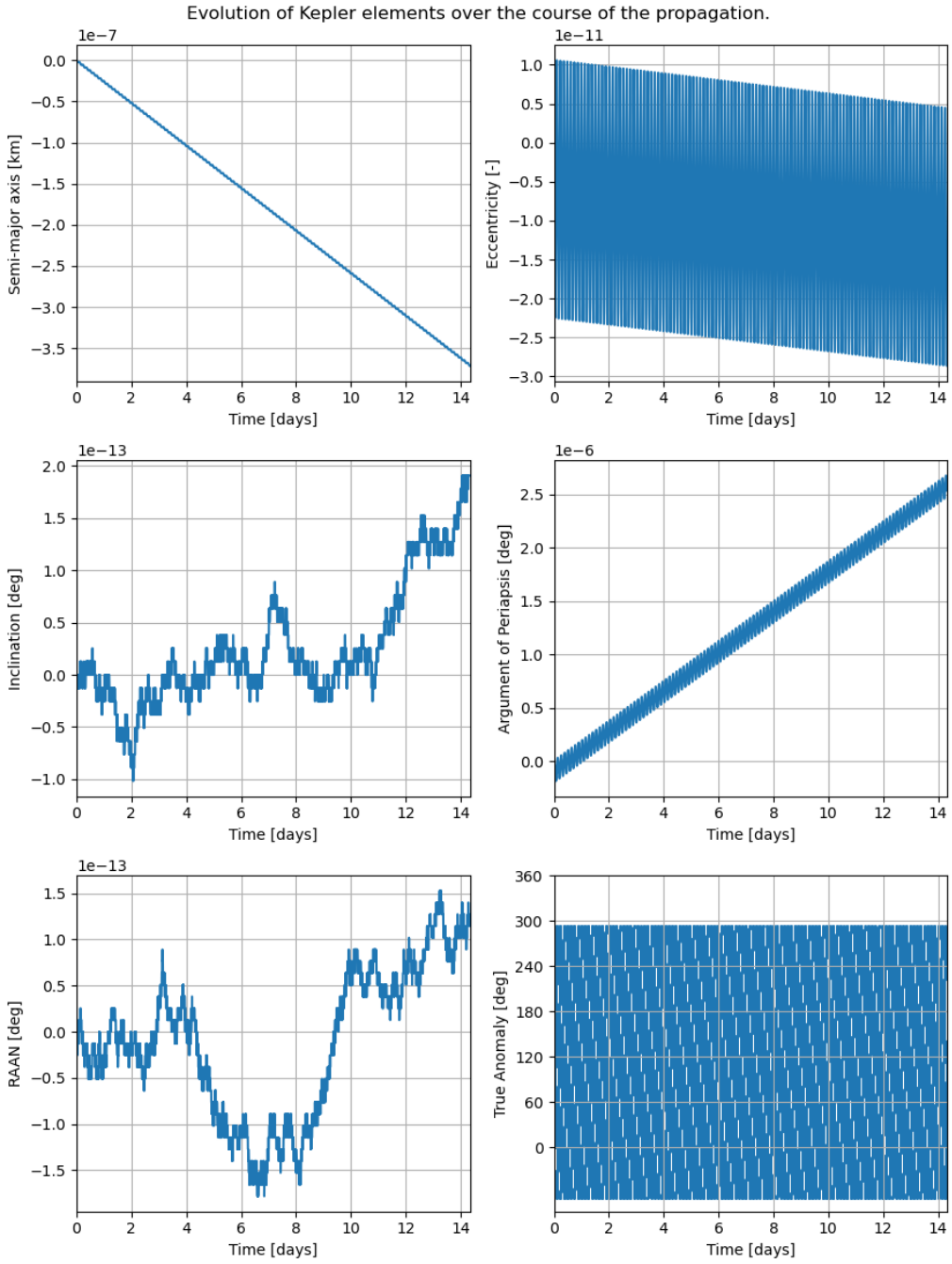

Figure 1.1: Change in Keplerian elements with respect to their value at t_0. Computed from the difference between the value at t and the value at $t0$.

1.2 Equations of Motion

$$(\vec{a}_s)_G = \frac{-\mu_G}{||\vec{r}_{G,s}||^3}\vec{r}_{G,s} \tag{1.1}$$

1.3 Environment Provided and Propagated Positions

The initial position of JUICE in the Ganymede-centered reference frame is provided by the environment based on the simulation_start_epoch. All other positions $\vec{r}_{G,s}$ are propagated with the 4th order Runge-Kutta method.

1.4 Analytical Solution of the Equation of Motion

Table 1.1: Name of symbols used throughout the assignment. Those are not repeated in subsequent questions.

Name	Symbol
Semi-major axis	a
True anomaly	θ
Eccentric anomaly	E
Mean anomaly	M
Argument of periapsis	ω
Right Ascension of the Ascending Node	Ω
Inclination	i
Eccentricity	e
Angular momentum vector	$\vec{h}$
Position vector	$\vec{r}$
Velocity vector	$\vec{V}$

$$\vec{r}_0 = \vec{r}_{G,s}|_{t_0} \qquad \vec{V}_0 = \vec{V}_{G,s}|_{t_0}$$

$$a = \frac{-\mu_G}{2\left(\frac{||V_0||^2}{2} - \frac{\mu_G}{||r_0||^2}\right)} \tag{1.2}$$

$$\vec{e} = \frac{1}{\mu_G}\left(\left(||\vec{V}_0||^2 - \frac{\mu_G}{||\vec{r}_0||}\right)\vec{r}_0 - (\vec{r}_0 \cdot \vec{V}_0)\vec{V}_0\right) \tag{1.3}$$

$$e = ||\vec{e}|| \tag{1.4}$$

$$\vec{h} = \vec{r}_0 \times \vec{V}_0 \tag{1.5}$$

$$i = \arccos\left(\frac{h_z}{||\vec{h}||}\right) \tag{1.6}$$

$$N = \begin{bmatrix}0\\0\\1\end{bmatrix} \times \vec{h} \tag{1.7}$$

$$\Omega = \arccos\left(\frac{N_X}{||\vec{N}||}\right) \tag{1.8}$$

$$\omega = \arccos\left(\frac{\vec{N} \cdot \vec{e}}{||\vec{N}||e}\right) \tag{1.9}$$

$$\theta = \arccos\left(\frac{\vec{e} \cdot \vec{r}_{G,s}}{e||\vec{r}_{G,s}||}\right) \tag{1.10}$$

Based on those analytical solutions, it is seen that all Keplerian elements, except the true anomaly, are expected to be constant. That is the case, because the solutions for a, ω, Ω, i, and e only depend on the initial state $\vec{r}_0$ and $\vec{V}_0$, whereas the true anomaly depends on the position vector $\vec{r}_{G,s}$ (which changes based on the Equation (1.1)). This is also seen from the plots shown in Figure 1.1, where the changes in a, ω, Ω, i, and e likely arise due to

numerical errors (very small changes over 344h), and the true anomaly varies by 360°over one orbit. Note that the change in ω is larger than for the other constant parameters: this is due to the link between the argument of periapsis and the true anomaly, hence the change in ω can be counteracted by a change in θ, and an error in θ of the order of 4.5e-6°is not unreasonable as it is varying (see Table 1.2). Furthermore, the numerical integration seems to predict an elliptic orbit, based on Figure 1.2, which is confirmed by the known analytical solution (Keplerian orbit: $||\vec{r}_{G,s}|| = \frac{a(1-e^2)}{1+e\cos\theta}$). Concluding, over the span of 344h, the Keplerian elements (for the given model) from the numerical integration are predicted with an accuracy of at least 8 orders of magnitude lower than the value considered, which is sufficient for most applications. Table 1.2 shows that the differences of the integrated and analytical values are small. The analytical value of θ at the end epoch was computed from,

$$\tan\left(\frac{\theta}{2}\right) = \sqrt{\frac{1+e}{1-e}}\tan\left(\frac{E}{2}\right) \qquad (1.11)$$

$$\sqrt{\frac{\mu_G}{a^3}}(t_{start} - t_{end}) = E - e\sin E \qquad (1.12)$$

Table 1.2: Comparison between the numerical (last data point) and analytical solutions. The analytical values were computed using μ_G from *bodies.get_body('Ganymede').gravitational_parameter*. The difference is given by TUDAT value - analytical value.

	a [km]	e [-]	i [°]	Ω [°]	ω [°]	θ [°]
TUDAT	≈ 3121.21	≈ 0.0092252	≈ 95.953	≈ 99.786	≈ 95.101	≈ 207.323
Analytical	≈ 3121.21	≈ 0.0092252	≈ 95.953	≈ 99.786	≈ 95.101	≈ 207.323
Difference	-3.7143e-07	-2.6868e-11	1.8474e-13	1.1369e-13	2.5340e-06	2.0224e-06

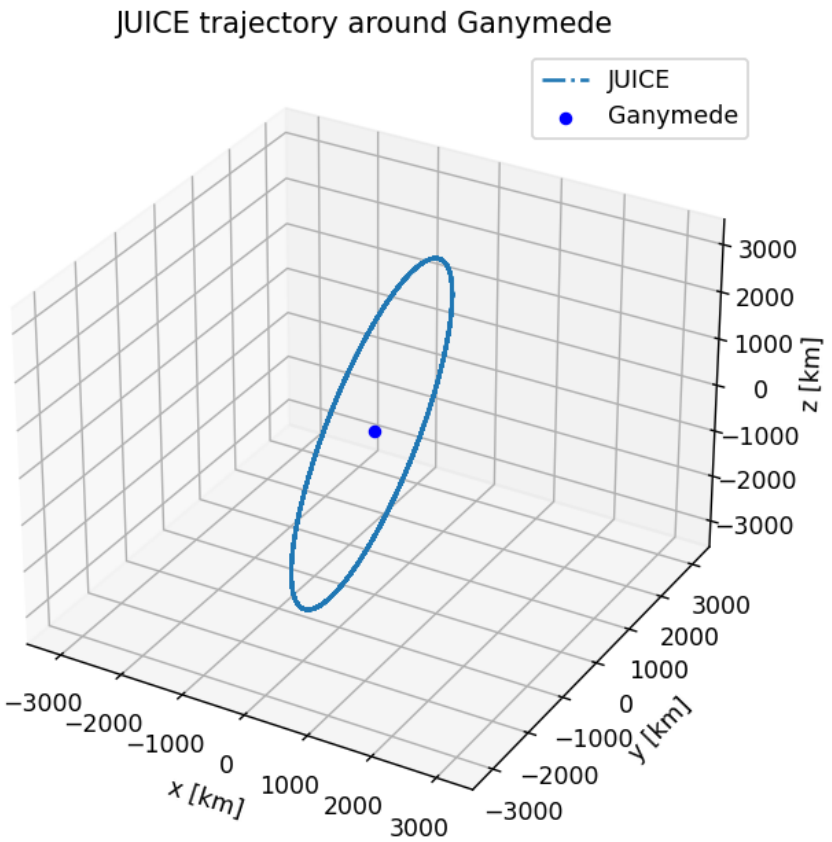

Figure 1.2: 3D plot of the propagated orbit.

Problem 2

2.1 Norm of Accelerations

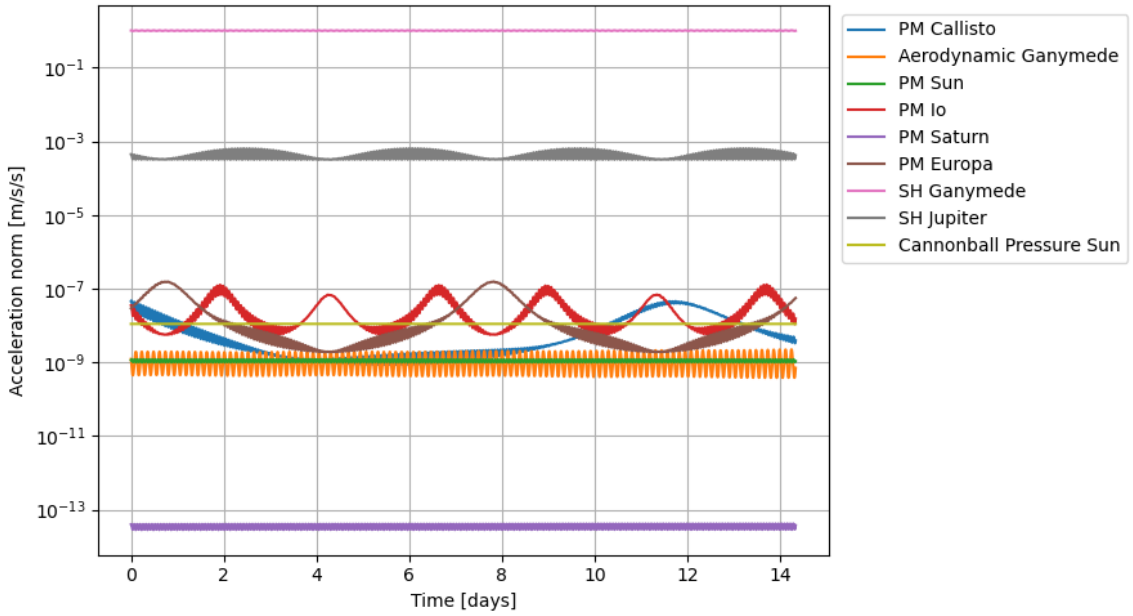

Figure 2.1: Accelerations norms on JUICE, distinguished by type and origin, over the course of propagation. PM=point mass gravity field, SH=spherical harmonics gravity field.

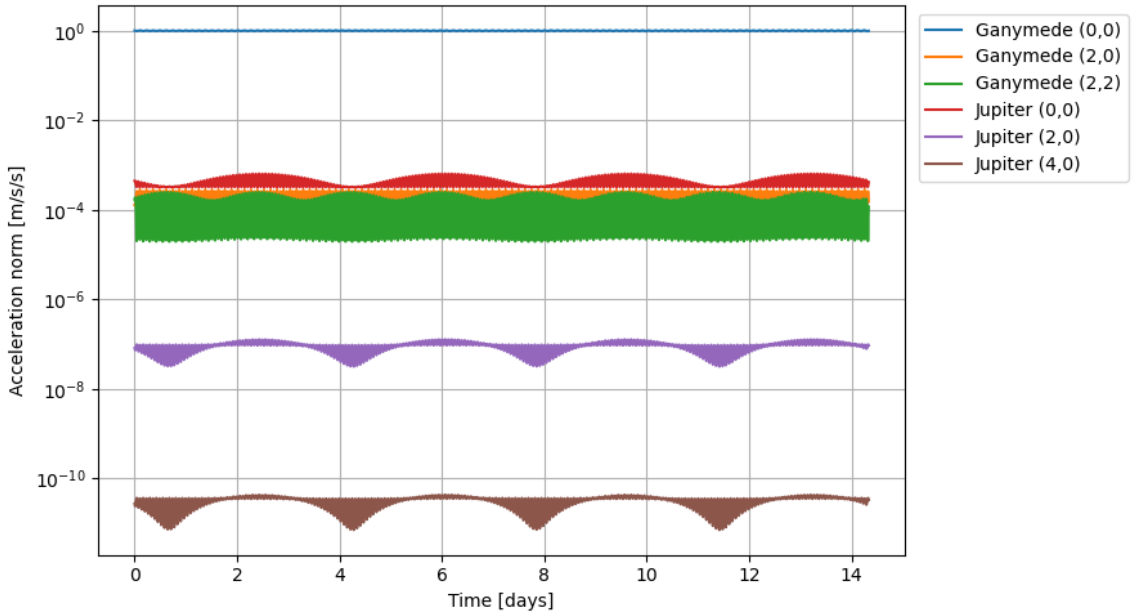

Figure 2.2: Spherical acceleration norms on JUICE, distinguished, over the course of propagation. (l,m): l=degree, m=order.

2.2 Formulation of the Gravitational Accelerations of Ganymede, Jupiter and Io on JUICE

Both Ganymede and Jupiter gravity fields are modelled using spherical harmonics and Io is modelled using a point mass. Ganymede is the central body, and Jupiter and Io are third body accelerations.

$$(\vec{a}_{G,s})_G = \nabla U_G(\vec{r}_{G,s}) \tag{2.1}$$

$$\begin{aligned}(\vec{a}_{J,s})_G &= \nabla U_J(\vec{r}_{J,s}) - \nabla U_J(\vec{r}_{J,G}) \\ &= \nabla U_J(\vec{r}_{J,G} + \vec{r}_{G,s}) - \nabla U_J(\vec{r}_{J,G})\end{aligned} \tag{2.2}$$

$$\begin{aligned}(\vec{a}_{I,s})_G &= \mu_I \left(\frac{\vec{r}_{I,G}}{||\vec{r}_{I,G}||^3} - \frac{\vec{r}_{I,s}}{||\vec{r}_{I,s}||^3} \right) \\ &= \mu_I \left(\frac{\vec{r}_{I,G}}{||\vec{r}_{I,G}||^3} - \frac{\vec{r}_{I,G} + \vec{r}_{G,s}}{||\vec{r}_{I,G} + \vec{r}_{G,s}||^3} \right)\end{aligned} \tag{2.3}$$

2.3 Environment Provided and Propagated Positions

Only $\vec{r}_{G,s}$ is numerically propagated in the simulation. The position vectors of Ganymede with respect to the other bodies $\vec{r}_{I,G}$ and $\vec{r}_{J,G}$ are retrieved from the environment using ephemerides.

2.4 Quasi-Periodic Variation of Gravitational Accelerations of the Sun and Io on JUICE

2.4.1 Norms

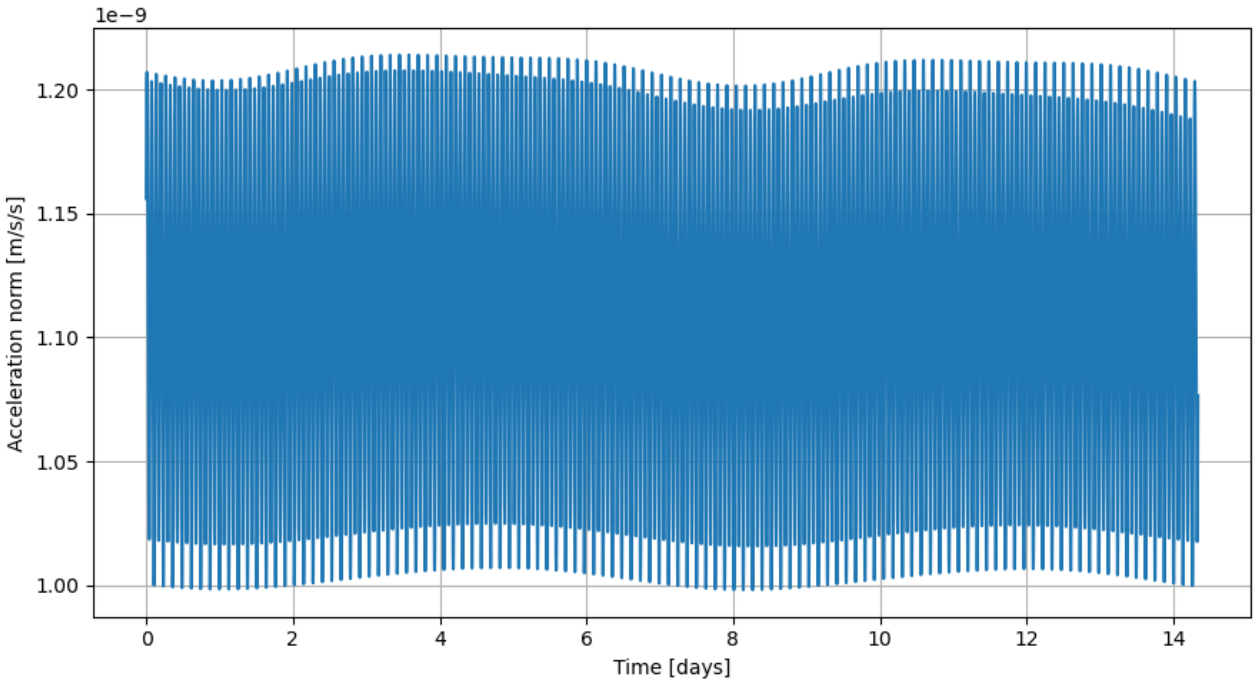

Figure 2.3: Norm of the gravitational acceleration from the point mass model of the Sun.

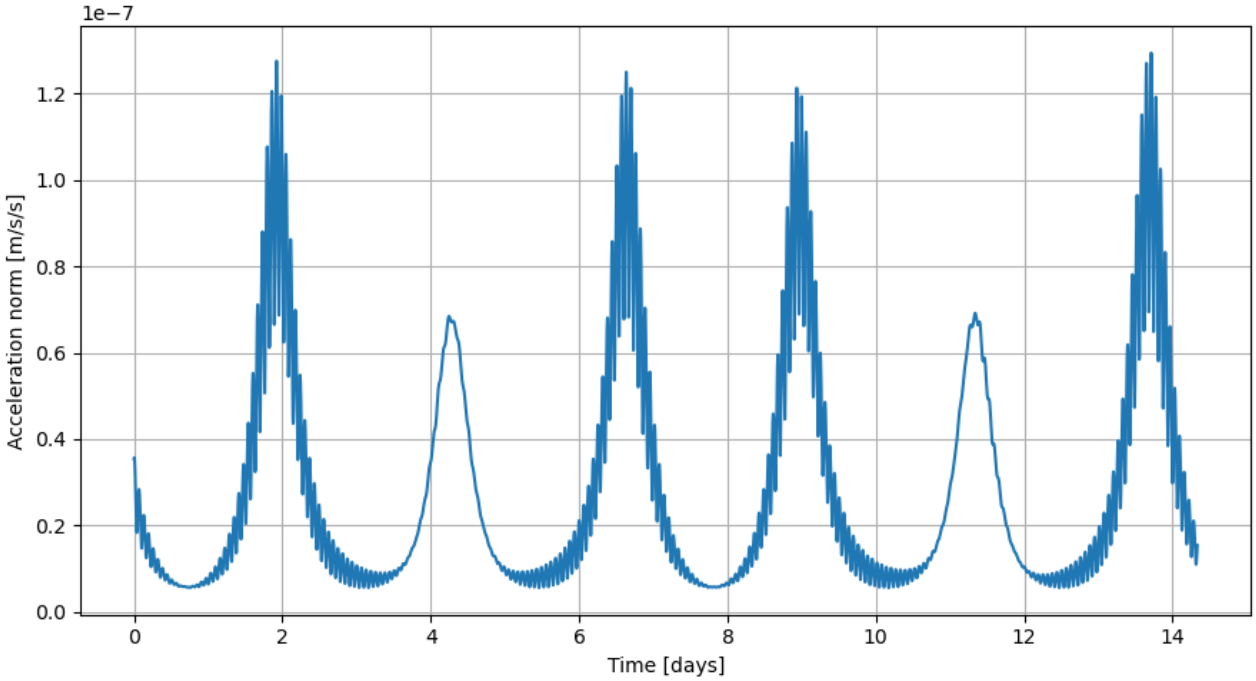

Figure 2.4: Norm of the gravitational acceleration from the point mass model of Io.

2.4.2 Period of Largest Amplitude

The period of largest amplitude is determined by using a Fast Fourier Transform (FFT) as implemented in the Scipy package. This permits an accurate estimation of the period and the method is highly reproducible. The result of the FFT are given in Figures 2.5 and 2.6. This gives $T_{ps} = 1.529$ hours (Sun case) and $T_{pi} = 57.334$ hours (Io case), where the exact values were retrieved numerically. Note that the zero frequency amplitude was removed while plotting as it does not relate to an oscillation.

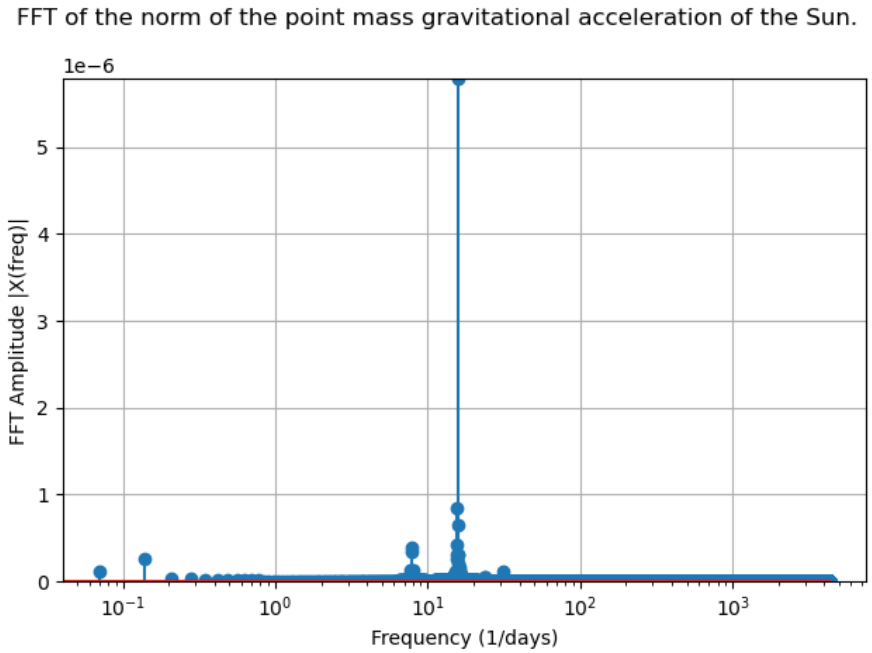

Figure 2.5: Fast Fourier Transform of the norm of the acceleration from the point mass gravitational model of the Sun.

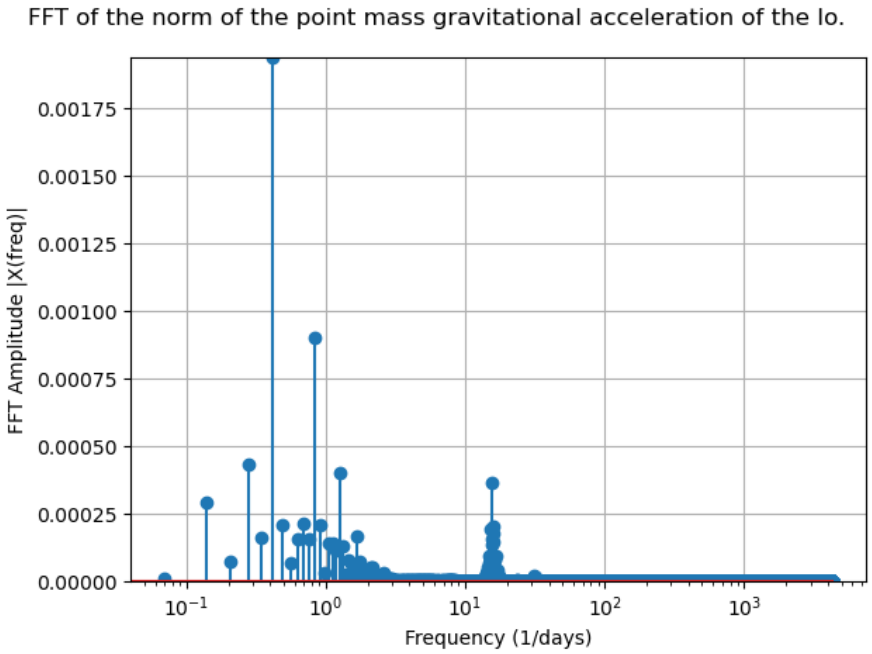

Figure 2.6: Fast Fourier Transform of the norm of the acceleration from the point mass gravitational model of Io.

2.4.3 Relating to Periods of the Bodies of the System

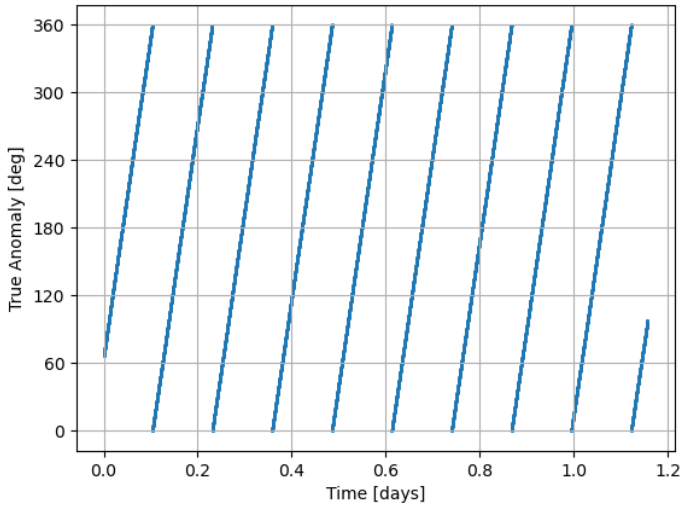

Figure 2.7: Plot of the true anomaly as a function of time. The orbital period of JUICE is estimated by considering one full sweep of the true anomaly.

Table 2.1: Orbital period of bodies in the system. Values taken from NASA fact sheets for planetary bodies.

Body	**Symbol**	**Value [days]**
Io	T_I	1.769138
Ganymede	T_G	7.154553
Jupiter	T_J	4,332.589
JUICE	T_{JUICE}	0.1274

$$T_{ps} \approx \frac{T_{JUICE}}{2} = 1.528h \qquad (2.4) \qquad\qquad T_{pi} \approx \frac{1}{\left|\frac{1}{T_G} - \frac{1}{T_I}\right|} = 56.407h \qquad (2.5)$$

The match is very accurate for Equation (2.4) and is off by about 1h (1.7%) for Equation (2.5).

2.5 Physical and Mathematical Reason

2.5.1 Sun Gravitational Perturbation

$$\vec{a}_{S,s} = \mu_S \left(\frac{\hat{r}_{S,G}}{||\vec{r}_{S,G}||^2} - \frac{\hat{r}_{S,G} + \hat{r}_{G,s}}{||\vec{r}_{S,G} + \vec{r}_{G,s}||^2} \right) \qquad (2.6)$$

The Sun perturbation is related to the difference in its attraction on JUICE and on Ganymede. With respect to the Sun, Ganymede and JUICE are very close to each other independently of their position in the solar system, meaning that the main oscillation arises from the movement of JUICE around Ganymede: in Equation (2.6), the change in direction of $\vec{r}_{G,s}$ gives rise to the largest oscillation, as $\vec{r}_{S,G}$ (relatively) does not vary much on 14 days. Assuming that over one period of JUICE, Jupiter and Ganymede do not move significantly ($\frac{T_{JUICE}}{T_J} = 0.0029\%$, $\frac{T_{JUICE}}{T_G} = 1.78\%$), Figure 2.8 is considered: cases (1) and (3) give rise to maxima as JUICE and Ganymede are stretched apart by the Sun ($\vec{r}_{S,G}$ and $\vec{r}_{S,s}$ are collinear); (2) and (4) give rise to minima as $\vec{r}_{S,G}$ and $\vec{r}_{S,s}$ are the most similar in this orientation. As exactly two maxima of the norm arise during one orbital period, the period of the largest oscillation is $\frac{T_{JUICE}}{2}$.

Figure 2.8: Sun 3rd-body acceleration diagram. Note that the orbit is not truthfully depicted.

2.5.2 Io Gravitational Perturbation

$$\vec{a}_{I,s} = \mu_I \left(\frac{\hat{r}_{I,G}}{||\vec{r}_{I,G}||^2} - \frac{\hat{r}_{I,G} + \hat{r}_{G,s}}{||\vec{r}_{I,G} + \vec{r}_{G,s}||^2} \right) \qquad (2.7)$$

Considering Equation (2.7), $\vec{r}_{I,G}$ changes the most (in magnitude), giving rise to the largest periodic variation in the 3rd body acceleration. This is due to the change in the relative position of Io and Ganymede over time, as seen from Figure 2.9 (assuming circular orbits in the same plane): $||\vec{r}_{I,G}||$ varies from $6.48e5$ to $1.488e6$ km (more than doubles)[1], and this variation is much larger than the one from $\vec{r}_{G,s}$. The period of the largest oscillation in the norm of the perturbation is then the time for the relative position of the two bodies to repeat: the synodic period for circular orbits in the same plane, given by Equation (2.5).

[1] https://nssdc.gsfc.nasa.gov/planetary/factsheet/galileanfact_table.html [Accessed on 02/03/2023]

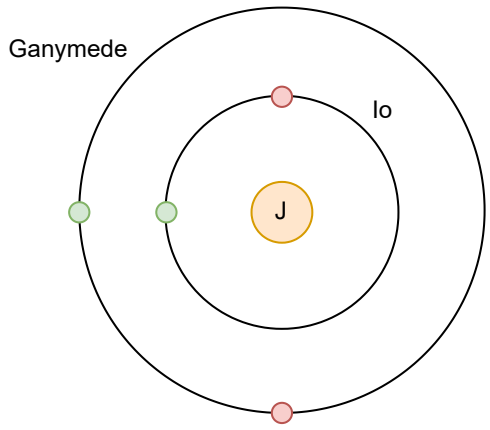

Figure 2.9: Io 3rd body perturbation diagram, assuming circular orbits of both Io and Ganymede. Green: maximum in disturbance, red: minimum in disturbance.

Problem 3

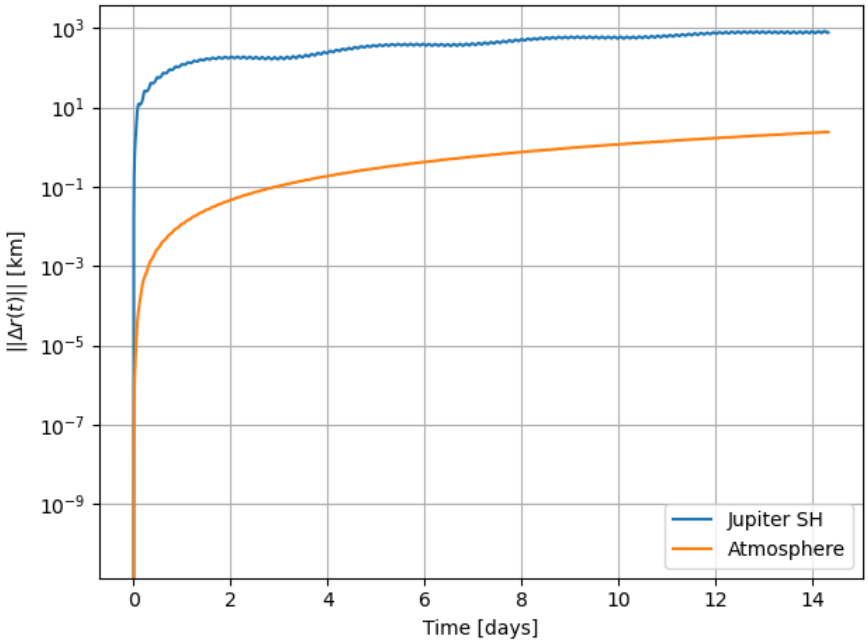

Figure 3.1: $||\Delta r(t)||$ for the aerodynamic and 3rd body spherical harmonics perturbations. SH=spherical harmonics. This result can be mainly attributed to the difference in orders of magnitude of the perturbations: the Jupiter SH acceleration is about 6 orders of magnitude larger than the aerodynamic acceleration.

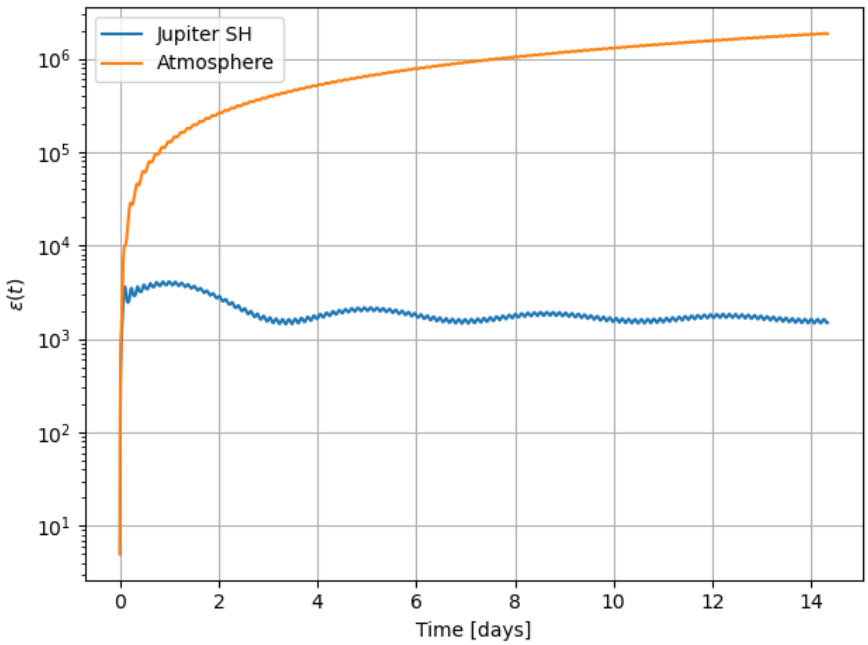

Figure 3.2: $\epsilon(t)$ for the aerodynamic and 3rd body spherical harmonics perturbations. SH=spherical harmonics.

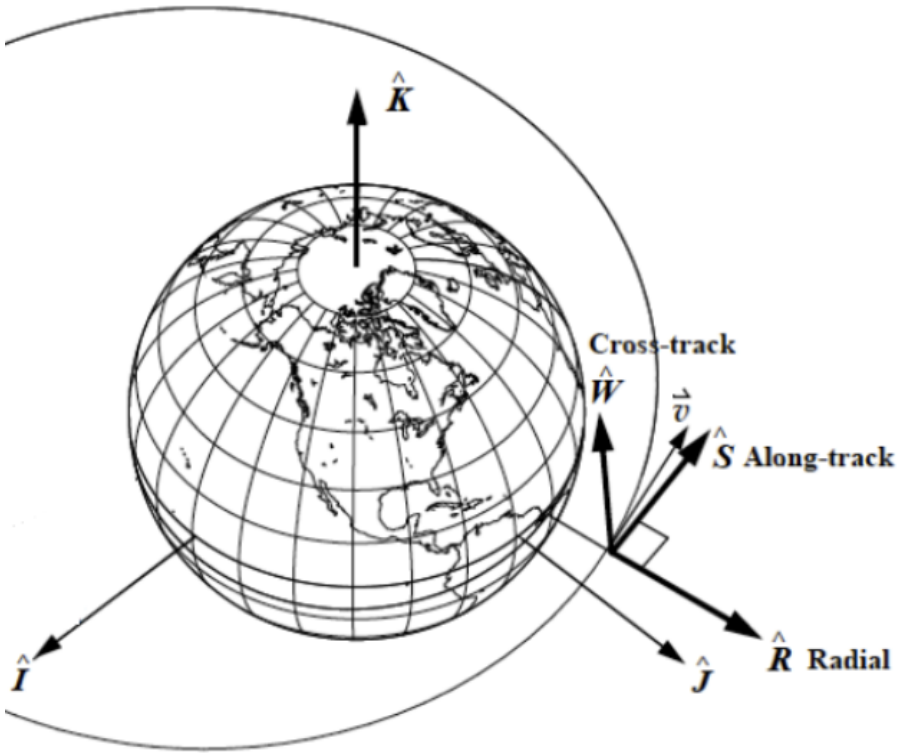

Figure 3.3: RSW satellite centred reference frame (around Earth but the exact same orientation applies around any body, taken from lecture slides).

From Figures 3.1 and 3.2, the Jupiter perturbation has the largest effect on the position, but the aerodynamic acceleration is the most effective because it acts **constantly** in the **negative along-track** direction. The effectiveness is linked to the behaviour of the acceleration in the RSW frame (Figure 3.3): (1) in (near-)circular orbits, the drag continuously acts in the along-track direction and opposite to the direction of motion with a nearly constant magnitude; (2) Jupiter's perturbation has components along all RSW directions depending on JUICE's position. Comparing constant accelerations of the same magnitude in each direction, the along-track perturbation was found (see lecture) to result in the largest change in Cartesian position (acts on the orbital energy), the other two being significantly less effective. Furthermore, the drag always acts in the same body-fixed direction: opposite to the direction of motion; while the Jupiter SH can act in opposite directions along the same RSW axis depending on the epoch (counter-acts itself), see Figure 3.4. The former is more 'efficient'.

Figure 3.4: Simple example of the attraction of Jupiter on JUICE having opposed effects at different orbital positions. Red arrow: acceleration, green arrow: orbital velocity at position. This means that the Jupiter acceleration can counter-act itself at different points along the orbit.

Problem 4

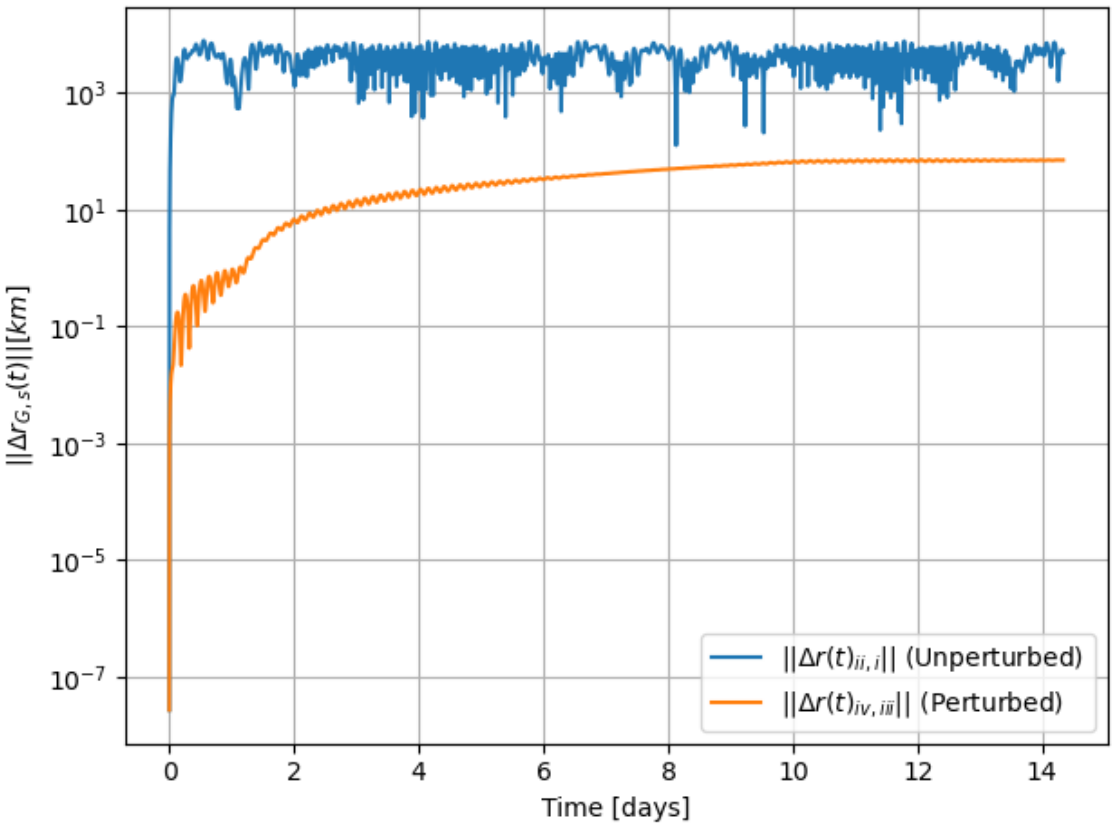

Figure 4.1: Norm of the difference Cartesian vector between Ganymede-centred and Jupiter-centred states.

4.1 Equations of Motion of JUICE in Jupiter-Centred Frame - Unperturbed Case

$$\begin{aligned}(\vec{a}_s)_J &= (\vec{a}_{J,s} - \underbrace{\vec{a}_{s,J}}_{\approx 0}) + (\vec{a}_{G,s})_J \\ &= \vec{a}_{J,s} + \mu_G \left(\frac{\vec{r}_{G,J}}{||\vec{r}_{G,J}||^3} - \frac{(\vec{r}_{G,J} + \vec{r}_{J,s})}{||\vec{r}_{G,J} + \vec{r}_{J,s}||^3} \right)\end{aligned} \tag{4.1}$$

4.2 Gravitational Acceleration of Io, Ganymede and Jupiter in Jupiter-Centred Frame - Perturbed Case

$$(\vec{a}_{J,s})_J = \nabla U_J(\vec{r}_{J,s}) \tag{4.2}$$

$$(\vec{a}_{G,s})_J = \nabla U_G(\vec{r}_{G,J} + \vec{r}_{J,s}) - \nabla U_G(\vec{r}_{G,J}) \tag{4.3}$$

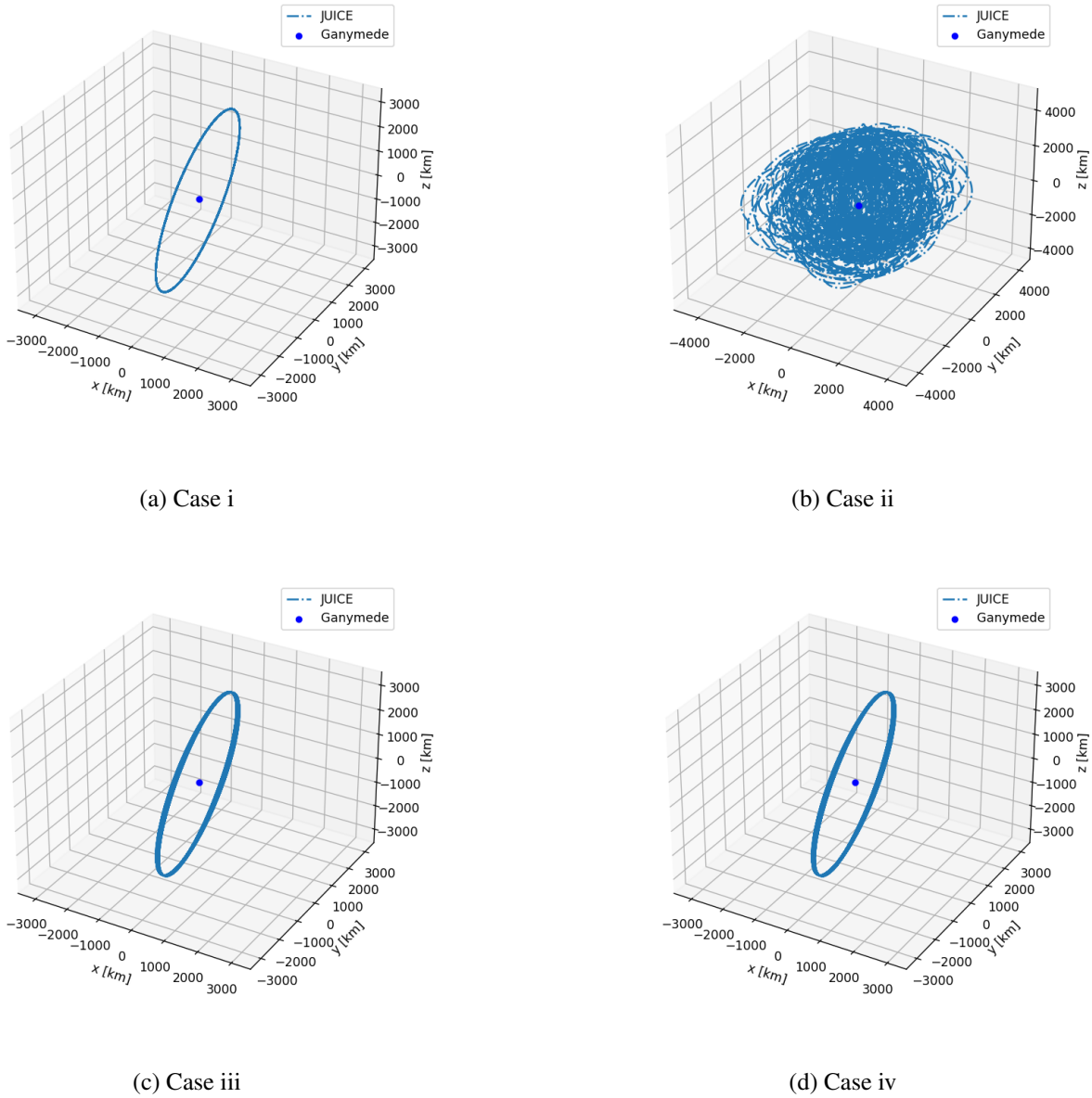

(a) Case i

(b) Case ii

(c) Case iii

(d) Case iv

Figure 4.2: 3D plots of JUICE's orbit around Ganymede for cases i, ii, iii, and iv

$$(\vec{a}_{I,s})_J = \mu_I \left(\frac{\vec{r}_{I,J}}{||\vec{r}_{I,J}||^3} - \frac{(\vec{r}_{I,J} + \vec{r}_{J,s})}{||\vec{r}_{I,J} + \vec{r}_{J,s}||^3} \right) \tag{4.4}$$

4.3 Effect of Changing the Centre of Propagation

The physics does not change (so the orbit should not change) when the centre of propagation is changed. Comparing the qualitative difference between cases i and ii, and cases iii and iv from Figure 4.1, it is clear that something goes wrong in the formulation of the equation of motion for case ii: Figure 4.2c is not similar to 4.2d. This is also confirmed by Figure 4.1, where $||\Delta r(t)_{ii,i}||$ is two orders of magnitude larger than $||\Delta r(t)_{iv,iii}||$.

In the unperturbed case, Equation (4.1) should be used (from theory) to propagate JUICE. The formulation treats Ganymede as a third body, and the acceleration of Jupiter on JUICE ($\vec{a}_{J,s}$) is required. Physically, the latter arises from the interaction of JUICE with the reference frame origin, $(\vec{a}_{J,s})_J$. However, defining Jupiter as the centre of propagation does not add Jupiter to the acceleration model, meaning that TUDAT takes $\vec{a}_{J,s} = 0$ in Equation (4.1). The acceleration of the propagation origin (Jupiter) on JUICE is neglected, resulting in an

incomplete model and an error in the propagation. In case iv, the acceleration of Jupiter is in the acceleration model, therefore, no such large propagation difference arises. Meaning that $||\Delta r(t)_{ii,i}|| >> ||\Delta r(t)_{iv,iii}||$.
The difference in Cartesian position of JUICE from cases iii and iv can be linked to the movement of Ganymede around Jupiter. In case iv, the orbit of Ganymede around Jupiter follows ephemeris data which was determined through n-body simulations, and is therefore predicted as if subjected to a more complete acceleration environment. Case iii uses a Ganymede-centred frame, meaning that the movement of Ganymede is not considered (only the relative position of other bodies are retrieved for 3rd body acceleration). Therefore, in case iii the ephemeris position of Ganymede has no effect on JUICE (only the acceleration model prescribed has an effect on its motion), whereas in case iv, JUICE orbits the position of the centre of mass of Ganymede as propagated in the ephemeris (from a different acceleration model) but is not subject itself to the more complete acceleration model. Hence, for case iv, we have Equation (4.5). This modelling difference yields $||\Delta r(t)_{iii,iv}|| > 0$.

$$\vec{r}_{G,s} = \underbrace{\vec{r}_{J,s}}_{\substack{\text{Propagated with specified} \\ \text{acceleration model}}} - \underbrace{\vec{r}_{J,G}}_{\substack{\text{Propagated with ephemerides} \\ \text{acceleration model}}} \tag{4.5}$$

4.4 Most Reliable Simulation

Case iii or iv are candidates due to the more complete acceleration models. Case iii is considered to be the most reliable, as it uses a variety of perturbation models and is Ganymede-centred (predicted motion of Ganymede does not impact JUICE's orbit). As seen above, case iv uses ephemerides for the motion of Ganymede, and hence uses two different acceleration models for JUICE and Ganymede, causing an inconsistency in Eq. (4.5): the propagation does not comply fully with the acceleration model specified and is less useful in mission design.

Problem 5

5.1 Thrust Law

Retrieved variables to evaluate the law (at time step): ω, θ, $\vec{r}$ and $\vec{V}$. The thrust is ON if JUICE is within 2°of θ of the ascending or the descending node. The inclination change is maximised by thrusting in the direction of the angular momentum vector, $\vec{h}$: out-of-plane direction, perpendicular to $\vec{V}$. In FoA, a component of $\Delta\vec{V}$ is in the velocity direction to ensure no change in other Keplerian elements. Here, those are allowed to change.

$$\theta_{AN} = 2\pi - \omega \tag{5.1}$$

$$\theta_{DN} = \pi - \omega \tag{5.2}$$

$$||\vec{T}|| = \begin{cases} 10\ N & \text{if } \theta_{AN} - 2° < \theta < \theta_{AN} + 2° \\ 10\ N & \text{if } \theta_{DN} - 2° < \theta < \theta_{DN} + 2° \\ 0\ N & \text{otherwise} \end{cases} \tag{5.3}$$

$$\hat{T} = \begin{cases} \frac{\vec{r}\times\vec{V}}{||\vec{r}\times\vec{V}||} & \text{if } \theta_{AN} - 2° < \theta < \theta_{AN} + 2° \\ -\frac{\vec{r}\times\vec{V}}{||\vec{r}\times\vec{V}||} & \text{if } \theta_{DN} - 2° < \theta < \theta_{DN} + 2° \\ \vec{0} & \text{otherwise} \end{cases} \tag{5.4}$$

5.2 Verification of the Implementation

5.2.1 ON/OFF Thrust

The thrust should be ON within 4°range of θ around each node. The nodes' true anomalies are found to be $\theta_{AN} \approx 269.27°$ (ascending) and $\theta_{DN} \approx 84.79°$ (descending) from Figure 5.1 (retrieved numerically). It is clear from Figure 5.3 that the thrust is ON in a region close to the nodes (where JUICE passes $z = 0$). Table 5.1 gives the theoretical and numerical θ ranges, showing slight differences because the algorithm is evaluated only every 10s. Therefore, if JUICE enters/leaves the 4°region, the engine is not ON/OFF until the next evaluation.

Table 5.1: Ranges of ON/OFF thrust settings according to the numerical result and the theoretical expectations.

Setting	θ **Range - Numerical**	θ **Range - Theoretical**
OFF	$0° \rightarrow 82.88°$	$0° \rightarrow 82.79°$
ON	$82.88° \rightarrow 86.85°$	$82.79° \rightarrow 86.79°$
OFF	$86.52° \rightarrow 267.35°$	$86.79° \rightarrow 267.27°$
ON	$267.35° \rightarrow 271.22°$	$267.27° \rightarrow 271.27°$
OFF	$271.22° \rightarrow 360°$	$271.27° \rightarrow 360°$

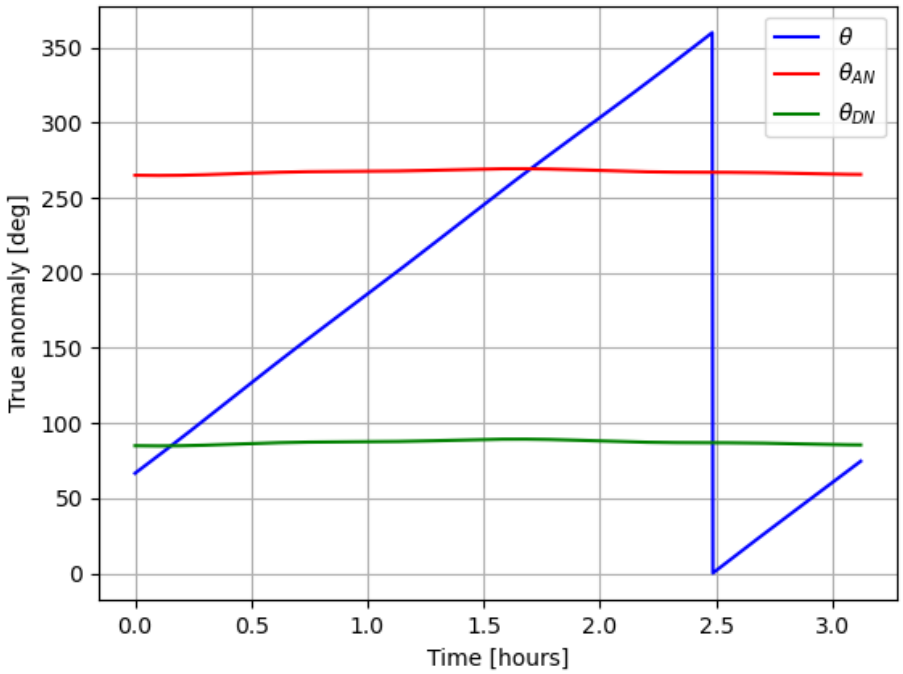

Figure 5.1: JUICE, and nodes true anomaly as a function of time. The relevant true anomaly of the ascending and descending nodes is determined based on the intersection of the θ curve with the curves of the true anomaly of each node (θ_{AN} and θ_{DN} change over time due to perturbations).

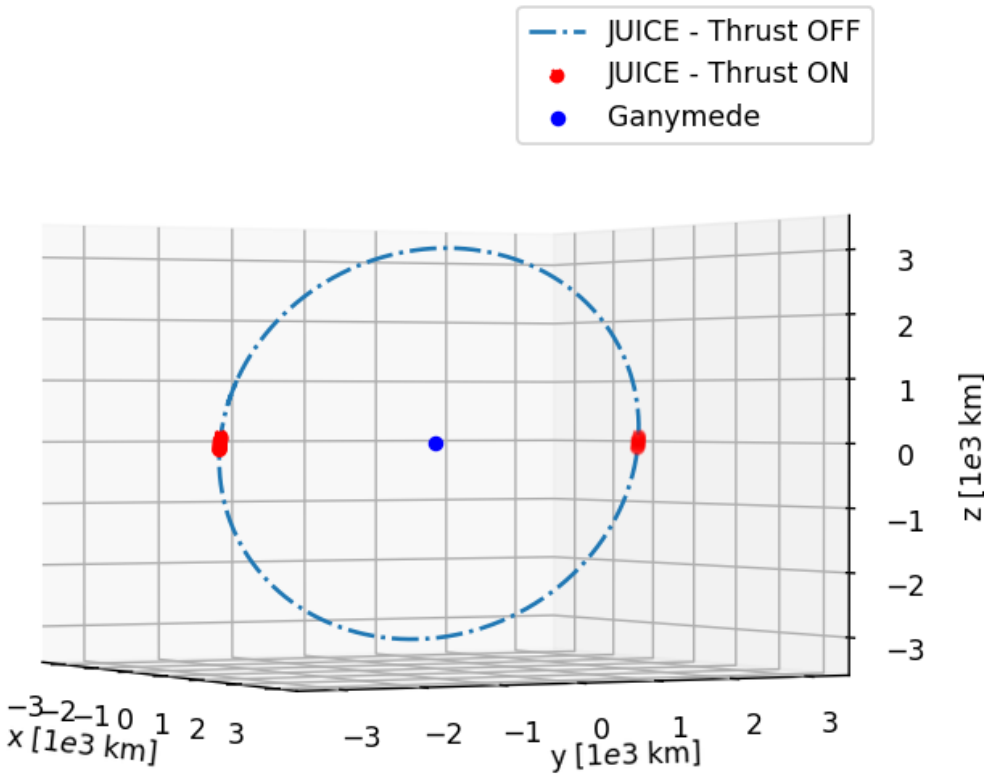

Figure 5.2: 3D plot of JUICE's first orbit since start epoch.

5.2.2 Mass Variation

JUICE's mass is expected to only change during the burns at the nodes. As the orbit is (near-)circular, each burn lasts for $t_{burn} = \frac{4T_{JUICE}}{360} \approx 122.3$s (4°sweep of θ, T_{JUICE} from Table 2.1), and the thrust is constant when ON: $\Delta m = \frac{||\vec{T}||t_{burn}}{I_{sp}g_0} = 0.4157$kg. Figure 5.3 indeed only shows a change in mass during burn and the propellant used during one node pass was found to be 0.4079kg (retrieved numerically). This difference between the theoretical and numerical values results from the time step size.

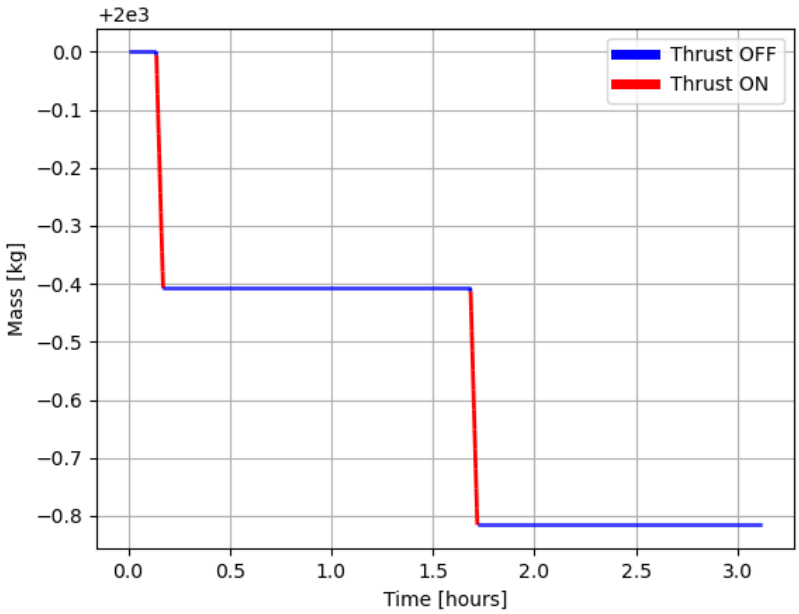

Figure 5.3: JUICE mass since start epoch.

5.2.3 Thrust Direction

For an impulsive manoeuvre, one burn is performed at the node in the direction of the angular momentum vector ($\vec{h}_{id}$). For the low-thrust manoeuvre, the direction of the thrust is adapted at each time step to be in the direction of $\vec{h}$, which changes due to the thrusting itself. Throughout the burn, the direction of the thrust vector then diverges from $\vec{h}_{id}$, see Figure 5.4. The difference in direction is given by the angle between the vectors,

$$\alpha = \arccos\left(\frac{\vec{h} \cdot \vec{h}_{id}}{||\vec{h}||||\vec{h}_{id}||}\right) \tag{5.5}$$

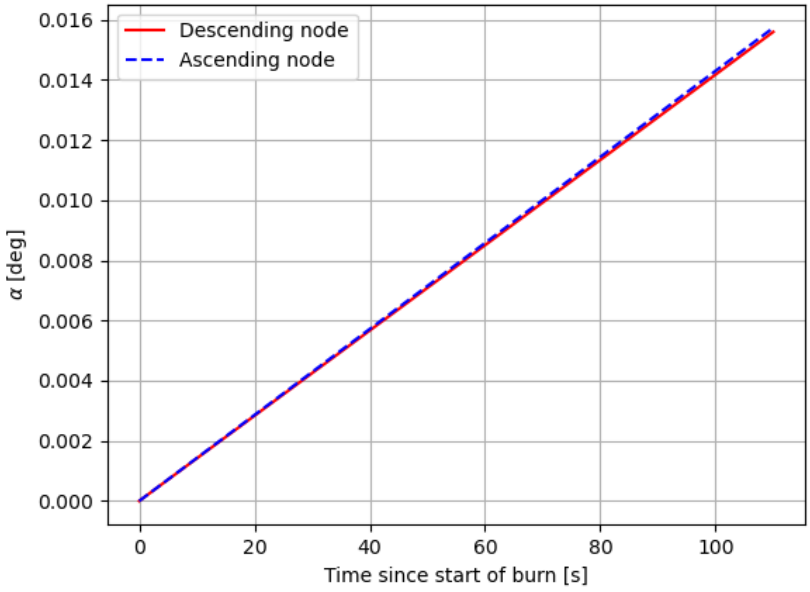

Figure 5.4: Thrust direction difference expressed as the angle α between the two vectors.

5.2.4 Inclination Change

For the theoretical expectations, the ideal ΔV achievable over the burn time of 122.3s (see above) is computed (Equations (5.6), (5.7)) and the associated Δi is obtained from Figure 5.5 and Equation (5.8), assuming an impulsive thrust ($\vec{V}_1$, the velocity before the burn from Figure 5.6). Figure 5.7 shows that the burns indeed increase the inclination in the simulation. Table 5.2 gives both the theoretical and numerical Δi over a complete burn, showing that the simulated Δi is 14-17% lower than the theoretical value obtained from an impulsive shot.

$$M_P = \frac{||\vec{T}||}{I_{sp} g_0} t_{burn} \tag{5.6}$$

$$\Delta V = I_{sp} g_0 \ln\left(\frac{M_{i,0}}{M_{i,0} - M_P}\right) \tag{5.7}$$

$$\Delta i = \arctan\left(\frac{\Delta V}{||\vec{V}_1||}\right) \tag{5.8}$$

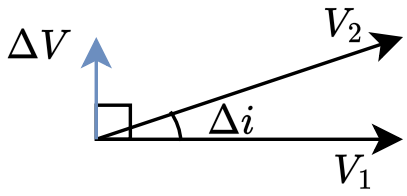

Figure 5.5: Inclination geometry.

Table 5.2: Inclination change on each burn. The difference arises mainly from the disturbances acting on JUICE during the manoeuvre (not impulsive).

	Numerical	**Theoretical**	**Difference**
First burn	0.01623°	0.01966°	17.44%
Second burn	0.01689°	0.01969°	14.22%

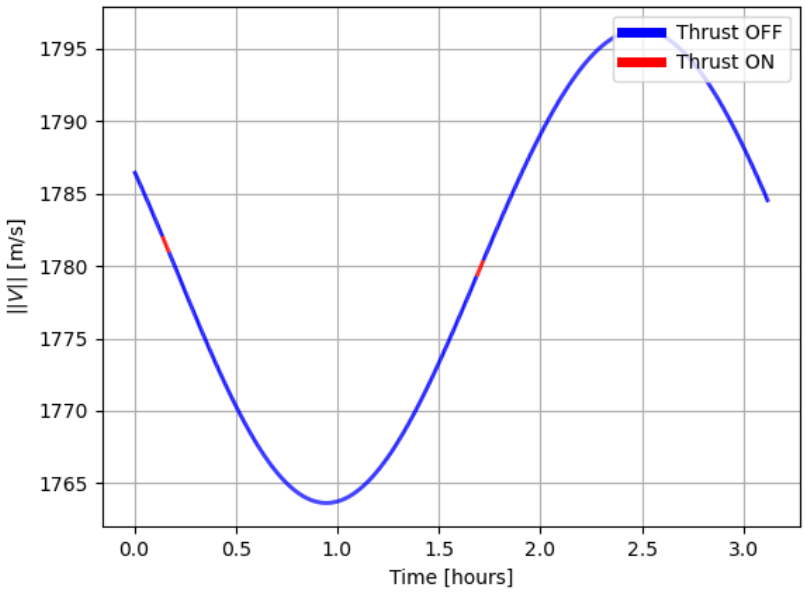

Figure 5.6: Norm of the velocity vector since start epoch. It can be seen that the thrust has only a limited effect on the velocity magnitude, as no sharp discontinuity is found.

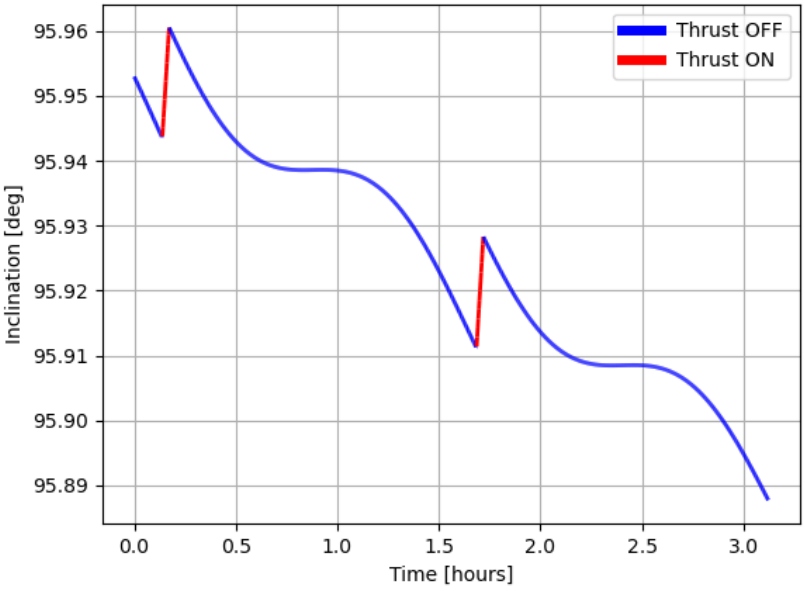

Figure 5.7: JUICE inclination since the start epoch. The overall trend of the inclination over this orbit is going down due to the external disturbances, but the trend on a longer period is going up due to the effects of the burns (as seen in the next section).

5.3 Effect on Keplerian Elements

From Figure 5.8, the overall inclination varies linearly with time (mass does not change much) and from Figure 5.9, it is found that the inclination changes sharply at each burn. As the burn periods are short compared to T_{JUICE}, the influence of thrust on inclination matches well the theoretical expectations.

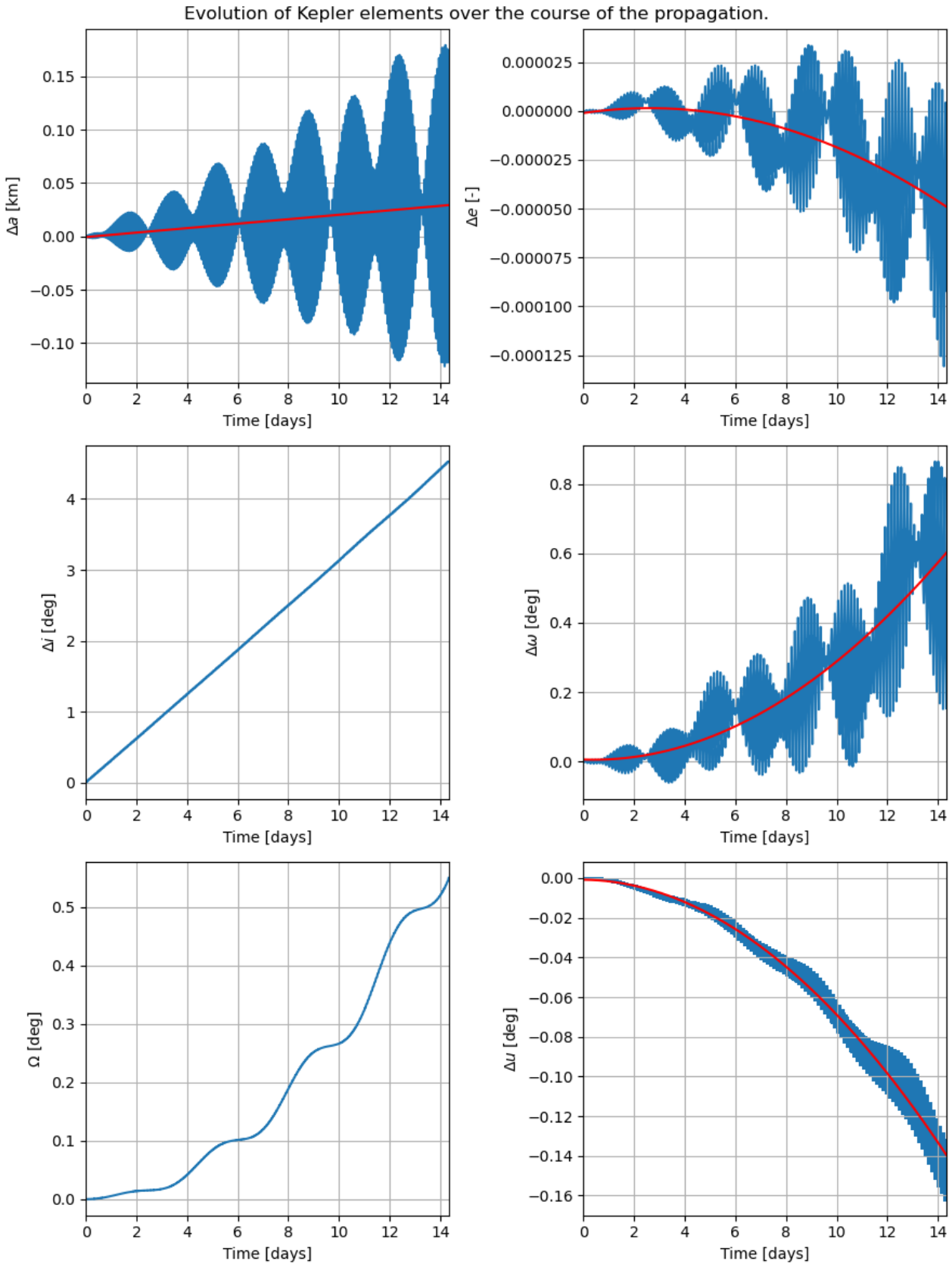

Figure 5.8: Change in the Keplerian Elements due to the thrust acceleration at the nodes. blue: complete change including the long- and short-period oscillations; red: secular trends in the value of the oscillating elements.

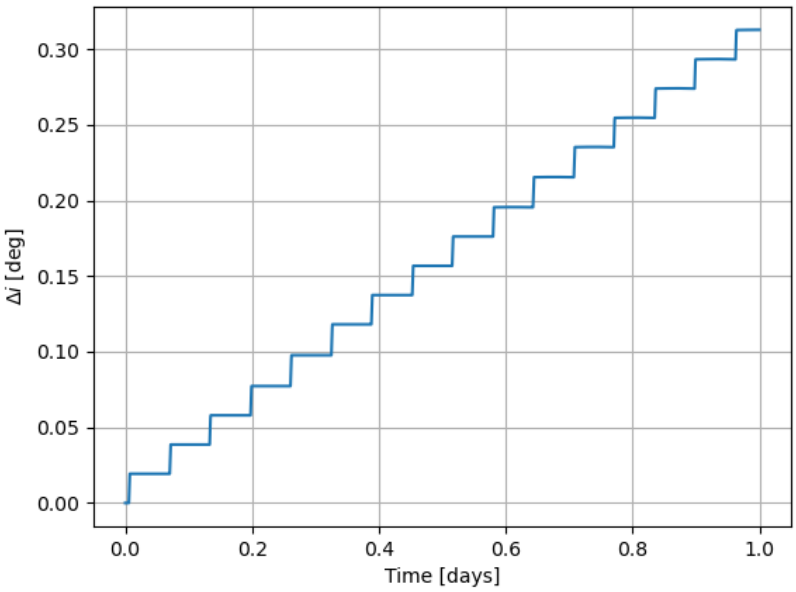

Figure 5.9: Inclination changes sub-structure.